



# Effect of pulse current on droplet transfer behavior and weld formation of 304 stainless steel in local dry underwater pulse MIG welding

Haipeng Liao<sup>1</sup> · Wenxu Zhang<sup>1</sup> · Xuyan Li<sup>1</sup> · Kai Pei<sup>1</sup> · Sanbao Lin<sup>2</sup> · Jiyu Tian<sup>1</sup> · Zhenmin Wang<sup>1</sup>

Received: 14 March 2022 / Accepted: 11 August 2022 / Published online: 17 August 2022  
© The Author(s), under exclusive licence to Springer-Verlag London Ltd., part of Springer Nature 2022

## Abstract

304 stainless steel, which is widely used in the industrial field due to its excellent thermostability, corrosion resistance, and welding performance, was welded using local dry underwater pulse metal inert gas (LDU-PMIG) welding technology in this study. The effect of different pulse peak currents on droplet transfer behavior and weld formation was investigated. The results show that short circuit transfer, globular transfer, and projected transfer were observed in the LDU-PMIG process. With the peak current of 240 A, the droplet transfer modes were short-circuit transfer and globular transfer; the weld formation was irregular with large particle spatters around the weld. With the peak current increased to 260 A, the droplet transfer mode changed into the globular transfer, and the weld formation quality was improved. With the peak current of 280 A, the droplet transfer mode was projected transfer, the weld formation was satisfied with a few spatters, and the coefficient of weld formation was the largest, and projected transfer was the most stable mode. With the increase of the peak current from 300 to 320 A, the droplet transfer mode did not change, but the instability of the welding arc resulted in poor weld formation with serious spatters and undercuts.

**Keywords** LDU-PMIG · 304 stainless steel · Peak current · Droplet transfer · Weld formation

## 1 Introduction

304 stainless steel exhibits the advantages of significant corrosion resistance and excellent mechanical property, which has been widely used in the marine environment, oil and gas industries, and nuclear sector [1]. Underwater welding is one of the most significant technology for the manufacturing and remanufacturing of 304 stainless steel structures in the marine equipment, including offshore drilling platform, marine engineering vessel, offshore wind power, and nuclear power plant [2]. Underwater welding technique mainly includes wet welding, dry welding, and local dry

welding [3]. Among them, local dry underwater welding (LDUW) has gradually become a research hotspot in the field of underwater welding due to high flexibility, good adaptability, low cost, and good weld formation [4, 5].

In the LDUW process, the drainage device is adopted to drain the water around the welding area to provide a stable local dry cavity for underwater welding, which is similar to the condition of on-land welding [6]. Recently, researchers have conducted a great deal of research on LDUW. Di et al. [7] used a drainage device to carry out welding experiments in LDUW successfully and concluded that the rapid cooling effect of underwater environment could improve the impact toughness and tensile strength of welds. Hu et al. [8] obtained duplex stainless steel welded joints under different simulated water depths by adopting local dry welding technique, and revealed that the austenite content of the weld joints increased initially and decreased afterwards. Han et al. [9] designed a micro-drain cover based on the shrinkage nozzle principle with a dual air curtain structure and carried out a series of experiments; they reported that the micro-drain cover could ensure the stability of welding process and the good quality of weld formation.

Pulse metal inert gas welding is an efficient welding method with low average input current, which is suitable

✉ Jiyu Tian  
tianjiyu@scut.edu.cn

✉ Zhenmin Wang  
wangzhm@scut.edu.cn

<sup>1</sup> School of Mechanical & Automotive Engineering, South China University of Technology, Guangzhou 510641, People's Republic of China

<sup>2</sup> State Key Laboratory of Advanced Welding and Joining, Harbin Institute of Technology, Harbin 150001, People's Republic of China

for all-directional welding of aluminum, magnesium, copper, and stainless steel, etc.; it can improve the stability of droplet transfer and obtain excellent weld formation. Hence, the combination of LDUW method and pulsed MIG technique (LDU-PMIG) has broad application prospect and important engineering application value.

Welding current has a significant impact on the welding process [10], which is mainly reflected in changing the heat input and the stability of welding process; these factors will greatly affect the quality of weld formation. Guo et al. [11] explored the effect of pulse current on the stability of welding process and weld formation in FCAW; they demonstrated that the stable mass transfer process and welding arc could increase the efficiency of heat input, decrease the acicular ferrite content, and increase the pre-eutectoid ferrite content in welds; the hardness and tensile strength of welds were similar to the in-air weld. Singh and Agrawal [12] studied the effect of welding current on the weld formation in tungsten inert gas welding. They put forward that with the increases of welding current, the weld penetration, weld width, and weld reinforcement all increased. Tabrizi et al. [13] researched the effect of pulse and continuous current on the mechanical performance of AISI 316L stainless steel joints in gas tungsten arc welding. They drew a conclusion that the welded joints under pulse current mode had higher hardness and toughness. Karunakaran and Balasubramanian [14] analyzed the effect of pulse current on the mechanical properties and microstructure characteristics of aluminum alloy joints welded by gas tungsten arc welding technique; they revealed that pulse current welding could improve the tensile strength of welds. However, researchers mainly focus on the analysis of weld formation quality for the effect of welding current on the welding process; few studies have concentrated on droplet transfer for that.

There are many modes of droplet transfer in MIG welding process; the transfer modes have a significant influence on weld formation quality [15, 16]. Therefore, researchers have conducted many studies on droplet transfer in welding process. Ma et al. [17] investigated the influence of the main arc voltage on arc behavior and droplet transfer in tri-arc twin wire welding. It indicated that with the increase of the main arc voltage, the droplet transfer changed from an unstable mixing transfer to a stable repulsion particle transfer. Wang et al. [18] explored the effect of ultra-high frequency on arc behavior and droplet transfer. Through experiments and theoretical analysis, they verified that ultra-high-frequency pulse alternating current cold metal transfer arc exhibited a good stability, with the pulse frequency increased from 60 to 80 kHz; the length of welding arc and the droplet diameter were maintained within an optimum range. Yang et al. [19] studied the influence of wire feeding speed on droplet transfer and weld formation in GMAW for high nitrogen austenitic stainless steel. The results revealed that stable

short circuit transfer, unstable short circuit transfer, and spray transfer would be observed in the process; the weld formation for stable short-circuit transfer was the best quality with few spatters. Cai [20] supplied Ar and He alternately as shielding gas in MIG welding for 5A06 aluminum alloy; they found that when the shielding gas was alternately supplied, the welding current fluctuated and the droplet transfer mode would change alternately. Wang et al. [21] studied the effect of pulse frequency on droplet transfer and weld formation in MIG welding. They demonstrated that with the increase of pulse frequency, the frequency of droplet transfer decreased. However, considering that changing pulse frequency during underwater welding will lead to the distortion of current waveform and discontinuity of heat input, the adjustment range of pulse frequency is narrow, which limits the control ability of pulse frequency for droplet transfer; it is not conducive to improve the weld formation quality. In the existing studies, there is little research about the effect of pulse peak current on droplet transfer behavior in the process of LDU-PMIG. Therefore, it is difficult to explain the effect of pulse current on the quality of weld formation from the perspective of droplet transfer behavior.

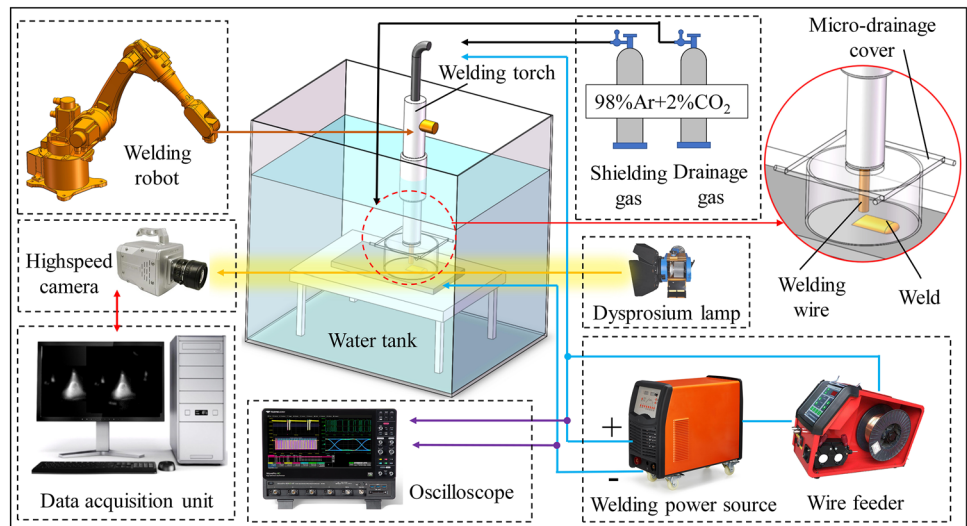
In this study, LDU-PMIG experiments were performed under different pulse currents, by collecting the electrical signals and droplet transfer images; the effects of pulse currents on droplet transfer and weld formation quality in the LDU-PMIG welding technique were investigated.

## 2 Experimental procedure

The test platform of LDU-PMIG is mainly composed of the welding robot, self-developed underwater welding power supply with the rated power of 15 kW, wire feeder, micro-drainage device, image capturing device, electrical signal acquisition device, and gas supply device, as shown in Fig. 1. Image capturing device includes the dysprosium lamp with the power of 1.8 kW and the high-speed camera with a frame rate of 2000 fps, which can be used to capture the images of droplet transfer during the welding process. The electrical signal acquisition device includes Hall sensor and oscilloscope, which can be adopted to detect welding current and voltage parameters during the welding process.

The welding material was AISI 304 stainless steel plate with a dimension of 300 mm × 100 mm × 5 mm. The welding wire was selected as 308Lsi with the diameter of 1.2 mm. To ensure the exploratory experiments under different pulse currents, parameters can be performed successfully, and multiple groups of pre-experiments were conducted. Considering the welding process stability and weld formation quality, the exploration range of peak current was set from 240 to 320 A. The welding robot was employed to perform the overlay welding experiments on

**Fig. 1** Schematic diagram of LDU-PMIG test platform



the stainless steel plate; the welding process was operated in a transparent water tank with a depth of 200 mm. The welding parameters are shown in Table 1. A mixed gas of 98% Ar and 2% CO<sub>2</sub> was used as the shielding gas and drainage gas. Compared with traditional on-land MIG welding, LDU-PMIG technique has a more complicated welding process due to the effect of rapid water cooling and larger gas flow. To avoid the huge interference of the complex underwater environment in the experiments, each group of pulse current parameters was carried out three times to reduce the errors.

After conducting the welding experiments, the electrical signals detected were processed to obtain the U-I diagrams; the stability of droplet transfer process was studied. The droplet transfer videos were edited into pictures to investigate the droplet transfer under different peak current parameters. A stereo microscope was adopted to detect the dimensions of the weld cross-section when the welds were cut, sampled, polished, and corroded. The corrosive solution was composed of picric acid, nitric acid, and ethyl alcohol. In addition, the mechanical model of droplet transfer was established to explain the formation mechanism for different droplet transfer modes and explore the influence of the droplet impact force on weld penetration.

### 3 Results and discussions

#### 3.1 Stability analysis of welding process

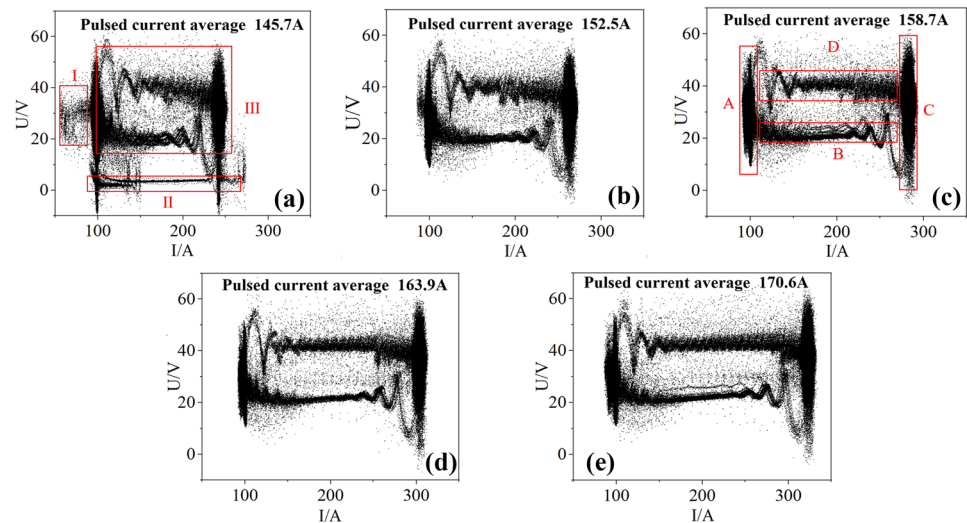
The U-I diagrams under each peak current were obtained as shown in Fig. 2. The trajectory of working points during the welding process can be clearly observed, and the concentration degree of working points can reflect the stability of welding current and voltage [22].

The U-I diagram of 240 A is illustrated in Fig. 2a; three typical arc state regions were observed, including arc-extinguishing region (I), short-circuit region (II), and arc-burning region (III). In arc-extinguishing region, the welding peak current was too inadequate to guarantee the stability of arc combustion. In short-circuit region, the droplet with welding wire was contacted with the molten pool before it separated from welding wire and caused the short circuit. At this moment, the arc voltage was small and the arc length was very short. The voltage detected was the output voltage of the welding power source, which was related to the welding wire, cable, and other resistances; therefore, the welding voltage would not reach 0. The occurrence of arc extinguishing and short circuit led to the extreme instability of the electrical parameters, which was

**Table 1** Parameters of welding test

Group	Base current (A)	Peak current (A)	Pulse frequency (Hz)	Peak current duty cycle	Welding speed (mm/s)	Drainage gas pressure (MPa)	Shielding gas pressure (MPa)
A	100	240	100	32%	15	0.2	0.2
B	100	260	100	32%	15	0.2	0.2
C	100	280	100	32%	15	0.2	0.2
D	100	300	100	32%	15	0.2	0.2
E	100	320	100	32%	15	0.2	0.2

**Fig. 2** a–e U-I diagrams of different peak currents



not conducive to the stable arc burning. The U-I diagram under 260 A is shown in Fig. 2b, the arc-extinguishing region and the short-circuit region disappeared, and the stability of welding process was improved. The U-I diagram of 280 A is shown in Fig. 2c. The welding voltage and current of the welding process had the least fluctuations, which indicates the arc stability of this parameter was the most satisfied. In the arc-burning region under this current, it could be observed that the U-I signal had an obvious circuit; A, B, C, and D regions were respectively the base current stage, the climbing stage from the base current to the peak current, the peak current stage, and the falling stage from the peak current to the base current. With the peak current increased from 300 to 320 A, the electrical parameters became unstable; that was because with the peak current increasing, the gap between the peak and base current became larger, and welding current frequently climbed vertically from the base current to the peak current, and then dropped vertically from the peak current to the base current, which would inevitably lead to violent fluctuations of welding arc.

### 3.2 Droplet transfer modes under different peak currents

Stable droplet transfer process is essential for high-stability welding process. Therefore, it is necessary to study the droplet transfer process under different peak current parameters and clarify the correlation systems between pulse currents and droplet transfer modes. With the peak current increased, three types of droplet transfer modes occurred in the welding process that were short circuit transfer, globular transfer, and projected transfer.

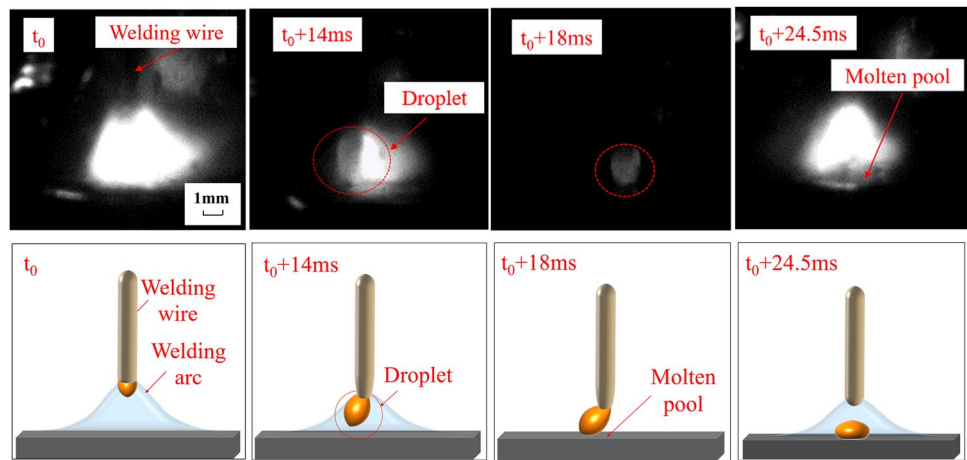
#### 3.2.1 Short circuit transfer

Small peak current leads to the insufficiency of heat input at the peak stage, resulting that the wire feeding speed is greater than the melting speed of welding wire; the droplet with the welding wire entered the molten pool early before separating from the welding wire. The whole process of droplet transfer takes place inside the molten pool, which forms the short-circuit transfer. When the peak current was 240 A, the droplet transfer modes were short-circuit transfer and globular transfer. The short-circuit transfer process is illustrated in Fig. 3. At the beginning, the welding wire was continuously fed into the molten pool, and no obvious droplet was observed at this moment. After 14 ms, a distinct droplet was developing, and then the droplet grew and began to approach the molten pool. At 18 ms, the welding wire with a large droplet contacted directly with the molten pool, which formed the short-circuit transfer. The arc voltage decreased rapidly and the arc light disappeared; only the appearance of the droplet could be observed, and the arc reignited at 24.5 ms. When short-circuit transfer was in process, the arc voltage decreased rapidly, while the welding current increased sharply. The whole process was matched with the electrical signal detected by acquisition system, as shown in Fig. 4; it is found that the electrical parameters under the short-circuit transfer mode were extremely unstable, and the current curve had a huge peak, which was not conducive to welding process.

#### 3.2.2 Globular transfer

When the peak current is small, the surface tension of the droplet prevents the droplet from separating from welding

**Fig. 3** Short circuit transfer process at the peak current of 240 A



wire, which results in metal accumulation at the root of the welding wire. At this moment, the droplet volume continuously increases. Then the droplet detaches from the welding wire under the action of gradually increasing gravity, which forms the globular transfer. Figure 5 illustrates the process of globular transfer with the peak current of 260 A. At the initial moment, it could be clearly observed that the droplet gradually grew at the root of the welding wire. The droplet began to separate from the wire at 5 ms, and then it kept a regular spherical shape. At 11 ms, the droplet transferred smoothly to the molten pool. At 15 ms, the droplet was contacted with the molten pool and the globular transfer process was completed. Figure 6 shows the output current and voltage waveforms of 260 A, the fluctuations of the electrical signals were slight, and the smooth globular droplet transfer mode can be obtained under this process parameter.

### 3.2.3 Projected transfer

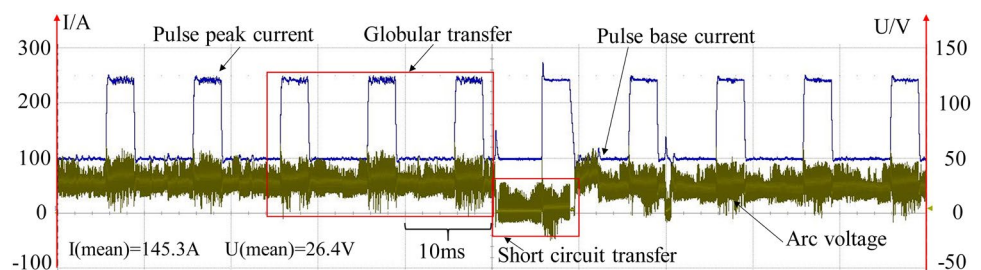
With the further increase of the peak current, the arc force generated by welding current makes the droplet separate from the welding wire before it grows, and the droplet shoots into molten pool at a high speed, which forms the projected transfer. When the peak current increased from 280 to 320 A, the droplet transfer mode was projected transfer. Figure 7 illustrates the whole process of droplet transfer with the peak current of 280 A. After separating from welding wire, the

overall shape of droplet was a regular ellipsoid. At 2 ms, it could be clearly observed that two droplets existed at the same time, and the droplets quickly dropped into the molten pool. It took 6 ms to complete the whole transfer process, which was generally the mode of many droplets in one pulse cycle. The diameter of the droplet was significantly decreased, and the dropping speed increased. According to the droplet transfer images and the output electrical signal waveforms of 280 A (Fig. 8), projected transfer was the most satisfied droplet transfer mode.

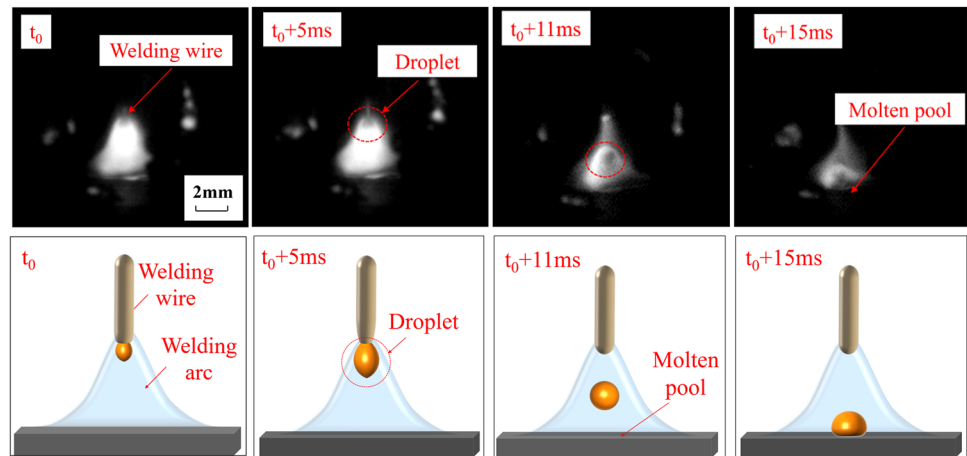
### 3.3 Weld formation characteristics

Figure 9 illustrates the weld formation of different peak currents. When the peak current was 240 A, the transfer mode was short-circuit transfer and globular transfer. Among them, the short-circuit transfer mode was extremely unstable, and droplet exploding would generate many explosive spatters during the transfer process, resulting in uneven weld formation with large particle spatters around the welds. With the peak current increased to 260 A, the short-circuit transfer disappeared, and the droplet transfer mode was globular transfer. Compared with short-circuit transfer, this mode was more stable. On the action of the arc force generated by welding arc, the droplet would deviate from the welding wire during the transfer process, causing that part of droplet to deviate from the molten pool, but the overall weld formation quality was improved. When the peak current was 280 A, the

**Fig. 4** The output current and voltage waveforms of 240 A



**Fig. 5** Globular transfer process with the peak current of 260 A



droplet transfer mode was projected transfer, and the droplet dropped into molten pool stably and quickly, which contributed to obtain high weld formation quality with satisfied continuity and smoothness. This droplet transfer mode was the most stable. When the peak current increased from 300 to 320 A, the transfer form was still projected droplet transfer. With the heat input further increased, the droplet dropping speed increased and the droplet diameter decreased. The instability of arc voltage caused irregular droplet dropping, which led to worse weld formation with some small particle spatters and undercuts.

Furthermore, to explore the influence of peak current on weld formation quality further, dimension detections were carried out on the cross-section of the welds; after the weld was sampled, the steel plate thickness of 5 mm was regarded as the calibration reference by using stereo microscope, the weld penetration ( $H$ ), weld width ( $B$ ), and weld reinforcement ( $h$ ) were obtained.

The coefficient of weld formation is the ratio of the weld width ( $B$ ) to the weld penetration ( $H$ ), which can be used to measure the weld formation quality. Three sets of sectional dimension data under each peak current parameter were detected and collected, and the average values and standard deviations of each sectional dimension were obtained. Figure 10 illustrates that with the increase of the

peak current, the weld width, weld penetration, and weld reinforcement increased, and the coefficient of weld formation first increased and then decreased. The coefficient of weld formation of 280 A was the largest. The error bar in Fig. 10 represented the standard deviation of each parameter. When the peak current was small, three unstable factors, including short circuit, arc interruption, and reignition, inevitably resulted in unstable droplet transfer. And with the peak current increased, the arc length increased, the droplet size decreased, and the dripping speed increased. Being subjected to the large arc force, the droplet transfer became disordered, which caused the inconformity of several sets of cross-sectional parameters of the same weld.

The increase of heat input would lead to the increase of weld penetration. But the strong water cooling effect caused by the contact between the rear face of base metal and water would lead to rapid cooling of the molten pool, which would inhibit the increase of weld penetration. In addition, the increase of the heat input would help to increase the weld width. However, with the increase of weld penetration, the arc length remained unchanged because the welding voltage did not change. When the arc dived into the molten pool, the decrease of arc swing angle would weaken the tendency increase of weld width and limit the growth speed of weld width. Besides, the increase of peak current made

**Fig. 6** The output current and voltage waveforms of 260 A

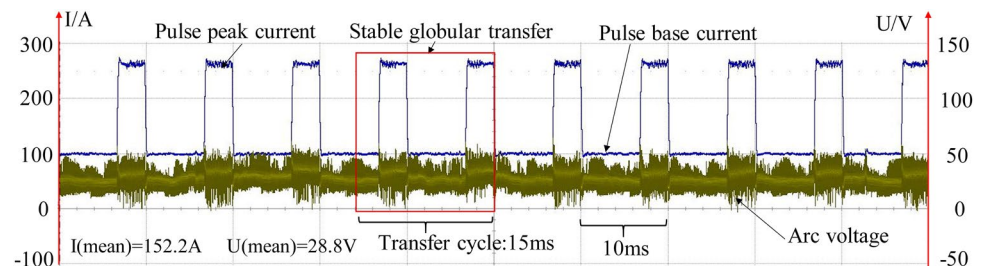
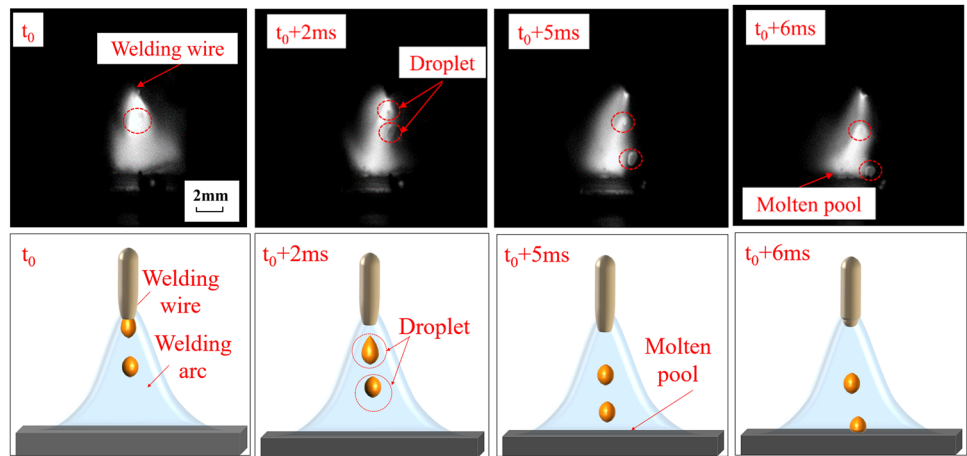


**Fig. 7** Projected transfer process with the peak current of 280 A



the increase of welding wire melting speed, which caused the increase of weld reinforcement accordingly. It could be found that with the current increased, the growth extent of weld width and weld penetration increased first and then decreased, for the reason that the increase extent of weld width was greater than that of weld penetration; the coefficient of weld formation increased initially and decreased afterwards.

### 3.4 Mechanical modelling and analysis of droplet transfer

#### 3.4.1 Formation mechanism of different droplet transfer modes

To profoundly explain the influence of different pulse currents on different droplet transfer modes, the mechanical model of droplet transfer was established and investigated. Figure 11 illustrates the mechanical model of the droplet growing at the root of welding wire. According to the static equilibrium theory [23], the droplet is subjected to gravity  $G$ , surface tension  $F_s$ , plasma flow force  $F_p$ , and electromagnetic force  $F_{em}$ . The direction of gravity, plasma force, and electromagnetic force is downward; these forces promote the droplet transfer into the molten pool, and the direction

of surface tension is upward, which maintains the droplet shape and prevents the droplet breaking away from the wire.

As the welding wire melting, the droplet grows gradually and causes the increase of droplet gravity. The calculation method of gravity is given by:

$$G = \frac{\pi D_0^3 \rho g}{6} \tag{1}$$

where  $D_0$  stands for the droplet diameter,  $\rho$  is the droplet density, and  $g$  represents the gravitational acceleration. Before separating from welding wire, the droplet is adhered to the welding wire due to surface tension, which is expressed as:

$$F_s = \pi d_0 \gamma \tag{2}$$

where  $d_0$  is the diameter of welding wire;  $\gamma$  is the surface tension coefficient. The coefficient will change with temperature, which depends on the welding current [24]. The relationship between surface tension coefficient  $\gamma$  and welding current  $I$  is expressed by:

$$\gamma = -0.0216 \times e^{\frac{I}{43.517}} + 4.11379 \tag{3}$$

Equation (3) reveals that with the increase of welding current, the surface tension coefficient decreases accordingly.

**Fig. 8** The output current and voltage waveforms of 280 A

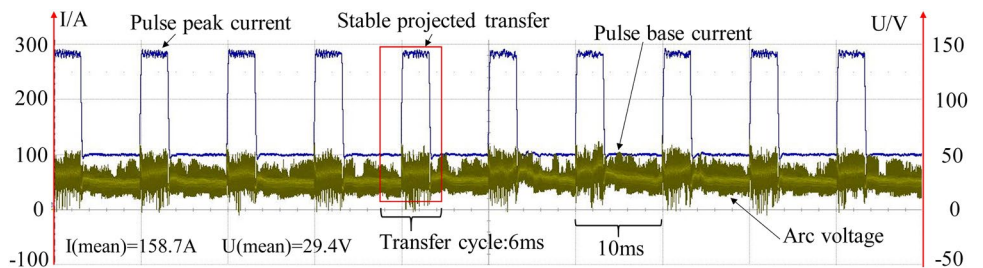
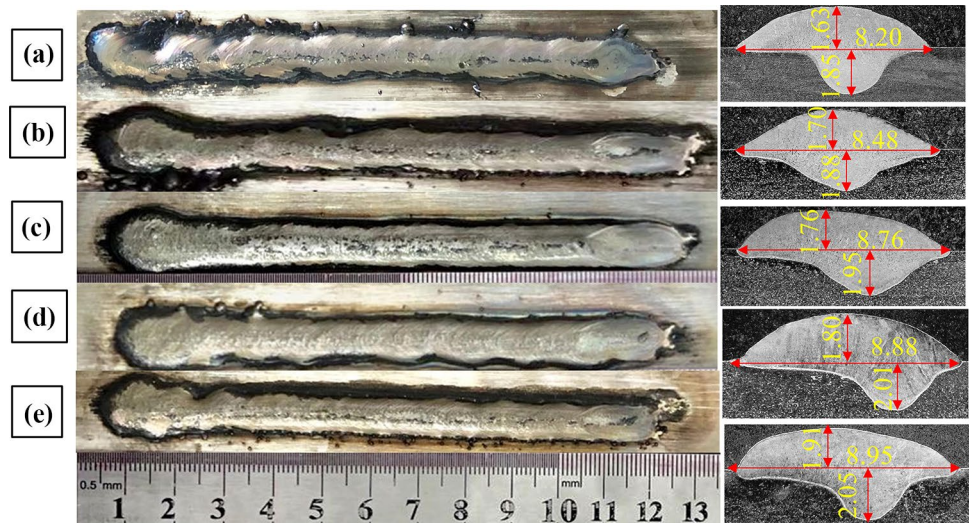


**Fig. 9** Weld formation and dimensions (unit: mm) of different peak currents: **a** 240 A; **b** 260 A; **c** 280 A; **d** 300 A; **e** 320 A



During the welding process, the conical welding arc makes the arc force different on the different section, resulting in a pressure difference. Axial thrust caused by the pressure difference prompts shielding gas to flow from the root of welding wire to the molten pool, forming the plasma flow force [25], which provides thrust to drive the droplet move towards the workpiece along the axis. The plasma flow force is expressed as:

$$F_p = A_p C_d \pi \frac{\rho_f v_f^2}{2} \tag{4}$$

where  $A_p$  is the action area of plasma flow force,  $C_d$  is the tension coefficient of plasma flow force, and  $\rho_f$  is the density of plasma that is the density of shielding gas;  $v_f$  is the plasma flow rate.

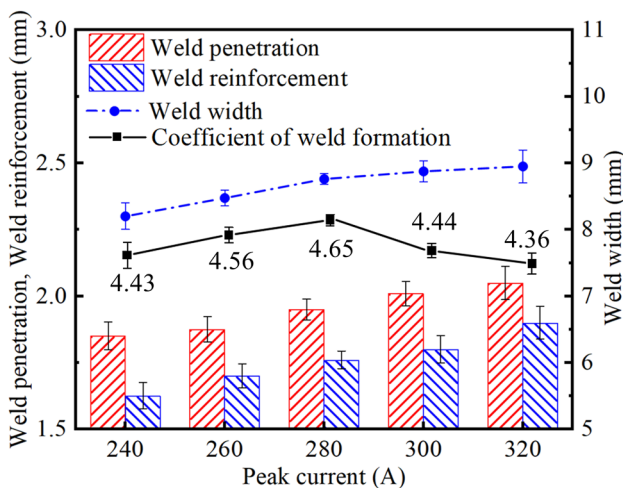


**Fig. 10** Weld dimensions of different peak currents

In the MIG welding process, electric field and magnetic field generated by the welding current flow will provide electromagnetic force  $F_{em}$  to the droplet, which is expressed as:

$$F_{em} = \frac{\mu_0 I^2}{4\pi} \left[ \ln \frac{D_0 \sin \theta}{d_0} + \frac{2}{(1 - \cos \theta)^2} \times \ln \frac{2}{1 + \cos \theta} - \frac{1}{1 - \cos \theta} - \frac{1}{4} \right] \tag{5}$$

where  $\mu_0$  is the vacuum permeability and  $\theta$  is the arc root angle.

The resultant force  $F$  on the droplet can be expressed as:

$$F = G + F_p + F_{em} - F_s \tag{6}$$

When the peak current is small, the surface tension  $F_s$  plays a dominant role in Eq. (6), causing that the resultant force  $F$  keeps less than 0, and the droplet cannot separate from the welding wire, which forms short-circuit transfer. With the peak current increases, the surface tension  $F_s$  decreases, and the welding wire melting prompts the droplet to develop adequately. At this time, the gravity  $G$  is in the leading position, making the resultant force  $F$  be more than 0; the droplet separates from the welding wire,

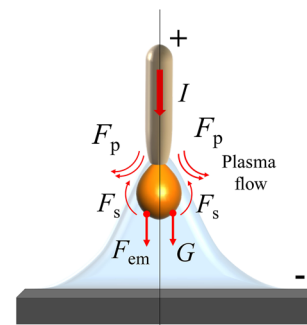


**Fig. 11** Mechanical model of droplet growth stage



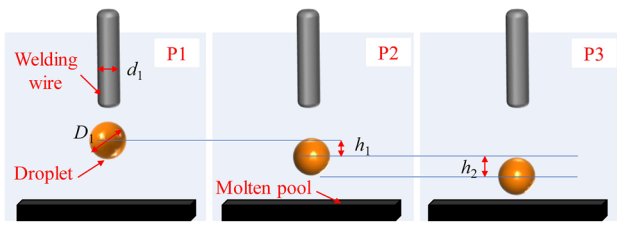


**Fig. 12** Solution schematic diagram of droplet diameter, velocity, and acceleration

which forms globular transfer. With the peak current further increasing, the electromagnetic force  $F_{em}$  increases a lot and becomes the most significant factor, causing the resultant force  $F$  be more than 0; the droplet detaches from the welding wire before it grows, which forms projected transfer.

**3.4.2 The effect of impact force on weld penetration**

To further explore the influence of peak current on weld penetration, it is necessary to calculate the momentum and impact force of the droplet before it falls into the molten pool. After the droplet transfer images were captured, the droplet diameters under different peak currents were calculated. Because of the same size of each picture, the welding wire diameter  $d_0$  of 1.2 mm was regarded as the reference substance.

As shown in Fig. 12,  $d_1$  and  $D_1$  stand for the welding wire diameter and droplet diameter measured by the picture, respectively; the actual droplet diameter  $D_0$  can be calculated:

$$D_0 = \frac{D_1 d_0}{d_1} \tag{7}$$

Then, the droplet mass  $m$  is expressed:

$$m = \frac{\pi \rho D_0^3}{6} \tag{8}$$

The high-speed camera was employed to capture the droplet transfer images with the frame rate of 2000 fps, and the time interval  $T$  of each picture was 0.5 ms, selecting three pictures of the droplet before falling into the molten pool, as shown in Fig. 12. According to the method of welding wire diameter reference, the displacement difference of three pictures were obtained as  $h_1$  and  $h_2$  respectively, and the velocity  $v$  and acceleration  $a$  of the droplet before entering the molten pool were approximately calculated by:

$$v = \frac{h_1 + h_2}{2T} \tag{9}$$

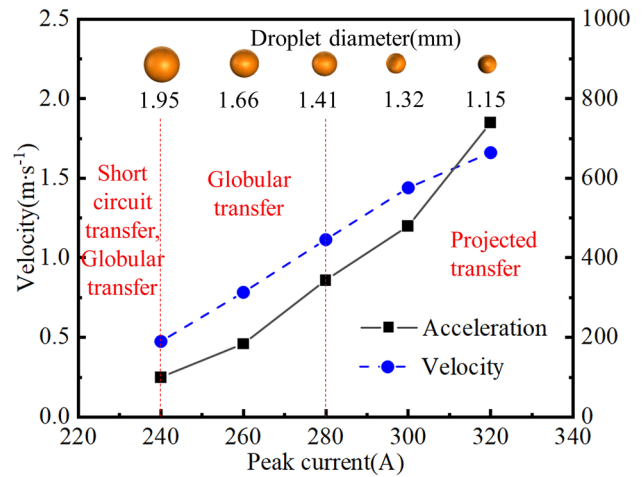


**Fig. 13** Droplet diameter, velocity, and acceleration of different peak currents

$$a = \frac{h_2 - h_1}{T^2} \tag{10}$$

According to Eqs. (7), (9) and (10), the actual diameter, velocity, and acceleration of the droplet under different peak currents were calculated, as shown in Fig. 13. It reveals that with the peak current increased, the diameter of the droplet decreased, and the speed and acceleration of the droplet increased.

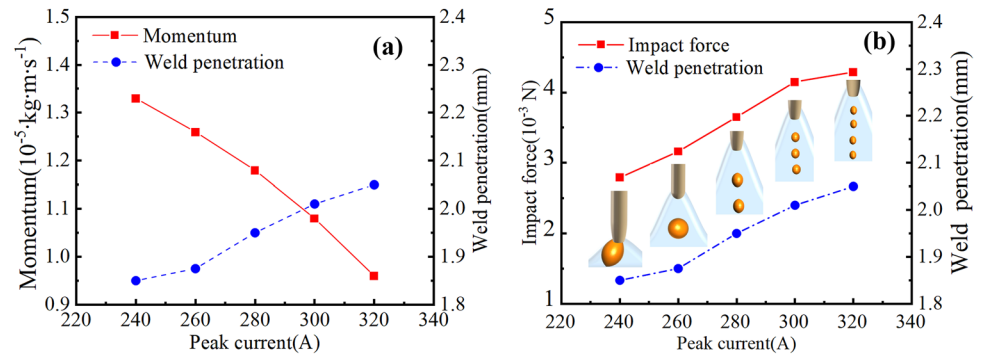
Then, the momentum  $p$  and the impact force  $Q$  of the droplet is expressed as:

$$p = mv = \frac{\pi \rho D_0^3 (h_1 + h_2)}{12T} \tag{11}$$

$$Q = ma = \frac{\pi \rho D_0^3 (h_2 - h_1)}{6T^2} \tag{12}$$

Figure 14 shows the effect of momentum and impact force of droplet on weld penetration under different peak currents. With the peak current increased, the droplet diameter decreased, and the droplet velocity increased; these two factors led to a decrease in droplet momentum. Figure 14a depicts that the weld penetration increased with the decrease of droplet momentum. It is obviously unreasonable to adopt droplet momentum as a reference for determining the weld penetration. Figure 14b illustrates that the impact force of droplet falling into the molten pool increased continually and had an evident positive effect on the weld penetration; that was, the greater the impact force, the deeper the weld penetration. Consequently, the droplet impact force can be regarded as the reference for determining the weld penetration.

**Fig. 14** Effect of momentum and impact force on weld penetration: **a** momentum; **b** impact force



## 4 Conclusions

In this study, several sets of LDU-PMIG welding experiments under different pulse currents (240 ~ 320 A) were conducted; the electrical parameters, droplet transfer images, and weld formation quality were investigated, then the mechanical model of the droplet transfer was established and investigated. The conclusions are summarized as follows:

1. With the increase of pulse peak current, the droplet transfer modes changed from short-circuit transfer and globular transfer (240 A) to globular transfer (260 A), then to projected transfer (280 ~ 320 A). Projected transfer was the most stable mode.
2. With the peak current of 280 A, the output electrical signals were ordered with the least fluctuates. The weld formation was satisfied with smoothness, uniformity, and absence of spatters and undercuts, and the coefficient of weld formation was the largest.
3. The mechanical model of droplet transfer revealed that with the peak current increased, the surface tension, gravity, and electromagnetic force would respectively take the leading place, which led to short-circuit transfer, globular transfer, and projected transfer, respectively.
4. With the peak current increased, the droplet diameter decreased, the droplet velocity and droplet impact force increased, but the droplet momentum decreased. The impact force had an extremely positive effect on the weld penetration, which could be adopted as the reference for determining the weld penetration.

**Acknowledgements** The authors are thankful to the editors and reviewers.

**Author contribution** The conceptualization and manuscript were conducted by Haipeng Liao. The experiments were designed by Wenxu Zhang, Xuyan Li, and Kai Pei; funding acquisition and manuscript review were performed by Sanbao Lin, Jiyu Tian, and Zhenmin Wang. All the authors took part in the paper.

**Funding** This work was supported by the National Natural Science Foundation of China (Grant number U2141216, Grant number 51875212); State Key Lab of Advanced Welding and Joining, Harbin Institute of Technology (Grant number AWJ21Z03, Grant number AWJ23M03); Key Technical Projects of Shenzhen City (Grant number JSGG20201201100401005, Grant number JSGG20201201100400001); Marine Economic Development (Six Marine Industries) Special Funding Project of Guangdong Province (Grant number GDNRC[2021]46); and Science and Technology Planning Project of Guangdong Province (Grant number 2021B1515420006); the International Cooperation Project of Guangzhou City (Grant number 201907010006).

**Data availability** The datasets generated and/or analyzed during the current study are available from the corresponding author on reasonable request.

## Declarations

**Ethics approval** Not applicable.

**Consent to participate** Not applicable.

**Consent for publication** Written informed consent for publication was obtained from all participants.

**Conflict of interest** The authors declare no competing interests.

## References

1. Li JZ, Sun QJ, Liu YB, Zhen ZY, Sun Q, Feng JC (2020) Melt flow and microstructural characteristics in beam oscillation superimposed laser welding of 304 stainless steel. *J Manuf Process* 50:629–637. <https://doi.org/10.1016/j.jmapro.2019.12.053>
2. Fu YL, Guo N, Cheng Q, Zhang D, Feng JC (2020) Underwater laser welding for 304 stainless steel with filler wire. *J Mater Res Technol* 9(6):15648–15661. <https://doi.org/10.1016/j.jmrt.2020.11.029>
3. Sehgal AK (2021) An investigation of variable welding current on impact strength of metal inert gas welded specimen. *Mater Today Proc* 37:3679–3682. <https://doi.org/10.1016/j.matpr.2020.10.151>
4. Sun K, Zeng M, Shi YH, Hu Y, Shen XQ (2018) Microstructure and corrosion behavior of S32101 stainless steel underwater dry and wet welded joints. *J Mater Process Tech* 256:190–201. <https://doi.org/10.1016/j.jmatprotec.2018.02.018>
5. Fydrych D, Rogalski G (2013) Effect of underwater local cavity welding method conditions on diffusible hydrogen content in

- deposited metal. *Weld Int* 27(3):196–202. <https://doi.org/10.1080/09507116.2011.600033>
6. Zhai YL, Yang LJ, He TX, Liu Y (2017) Weld morphology and microstructure during simulated local dry underwater FCTIG. *J Mater Process Tech* 250:73–80. <https://doi.org/10.1016/j.jmatprotec.2017.07.010>
  7. Di XJ, Ji SX, Cheng FJ, Wang DP, Cao J (2015) Effect of cooling rate on microstructure, inclusions and mechanical properties of weld metal in simulated LDUW. *Mater Des* 88:505–513. <https://doi.org/10.1016/j.matdes.2015.09.025>
  8. Hu Y, Shi YH, Sun K, Shen XQ (2019) Microstructure evolution and mechanical performance of underwater local dry welded DSS metals at various simulated water depths. *J Mater Process Tech* 264:366–376. <https://doi.org/10.1016/j.jmatprotec.2018.09.023>
  9. Han LG, Wu XM, Chen GD, Wang ZM, Fan WY (2019) LDUW of 304 stainless steel based on a microdrain cover. *J Mater Process Tech* 268:47–53. <https://doi.org/10.1016/j.jmatprotec.2018.12.029>
  10. Shi YH, Wang GR (2006) Vision based seam tracking system for underwater flux cored arc welding. *Sci Technol Weld Join* 11(3):271–277. <https://doi.org/10.1179/174329306x102084>
  11. Guo N, Cheng Q, Fu YL, Du YP, Zhang X, Feng JC (2019) Investigation on the mass transfer control, process stability and welding quality during underwater pulse current FCAW for Q235. *J Manuf Process* 46:317–327. <https://doi.org/10.1016/j.jmapro.2019.08.022>
  12. Singh RP, Agrawal MK (2021) Effect of welding current on the dimensions of bead in tungsten inert gas welding process. *Mater Today Proc* 45:3235–3239. <https://doi.org/10.1016/j.matpr.2020.12.382>
  13. Tabrizi TR, Sabzi M, Anijdan SHM, Eivani AR, Park N, Jafarian HR (2021) Comparing the effect of continuous and pulsed current in the GTAW process of AISI 316L stainless steel welded joint: microstructural evolution, phase equilibrium, mechanical properties and fracture mode. *J Mater Res Technol* 15:199–212. <https://doi.org/10.1016/j.jmrt.2021.07.154>
  14. Karunakaran N, Balasubramanian V (2021) Effect of pulsed current on temperature distribution, weld bead profiles and characteristics of gas tungsten arc welded aluminum alloy joints. *Trans Nonferr Metal Soc* 21:278–286. [https://doi.org/10.1016/S1003-6326\(11\)60710-3](https://doi.org/10.1016/S1003-6326(11)60710-3)
  15. Kang S, Kang M, Jang YH, Kim C (2020) Droplet transfer and spatter generation in DC–AC pulse tandem gas metal arc welding. *Sci Technol Weld Join* 25(7):589–599. <https://doi.org/10.1080/13621718.2020.1786262>
  16. Cai XY, Fan CL, Lin SB, Yang CL, Ji XR, Hu L (2016) Effects of shielding gas composition on arc characteristics and droplet transfer in tandem narrow gap GMA welding. *Sci Technol Weld Join* 22(5):1–8. <https://doi.org/10.1080/13621718.2016.1253535>
  17. Ma Z, Zhuang MH, Li MQ (2020) Effect of main arc voltage on arc behavior and droplet transfer in tri-arc twin wire welding. *J Mater Res Technol* 9(3):4876–4883. <https://doi.org/10.1016/j.jmrt.2020.03.007>
  18. Wang DL, Wu CF, Suo YC, Wang LW, Liang ZM (2019) Effect of pulse frequency on arc behavior and droplet transfer of 2198 Al–Li alloy by ultrahigh-frequency pulse AC CMT welding. *J Mater Res Technol* 8(5):3950–3958. <https://doi.org/10.1016/j.jmrt.2019.07.003>
  19. Yang DQ, Xiong HY, Huang Y, Yan DJ (2021) Droplet transfer behavior and weld formation of gas metal arc welding for high nitrogen austenitic stainless steel. *J Manuf Process* 65(3):491–501. <https://doi.org/10.1016/j.jmapro.2021.03.048>
  20. Cai XY, Lin SB, Wang BZ (2020) Droplet transfer and weld formation of MIG welding with Ar–He alternating gas for aluminum alloy. *J Manuf Process* 49:94–101. <https://doi.org/10.1016/j.jmapro.2019.11.012>
  21. Wang ZM, Pei K, Han LG, Wu HD, Lin SB, Cai XY, Xu MJ, Zhang Q (2021) Effect of pulse frequency on droplet transfer and weld formation in local dry underwater welding. *J Manuf Process* 68:1726–1734. <https://doi.org/10.1016/j.jmapro.2021.06.065>
  22. Ma Q, Luo CC, Liu SX, Li HL, Wang PF, Liu D, Lei YC (2021) Investigation of arc stability, microstructure evolution and corrosion resistance in underwater wet FCAW of duplex stainless steel. *J Mater Res Technol* 15:5482–8492. <https://doi.org/10.1016/j.jmrt.2021.11.023>
  23. Zhang SY, Ma GH, Peng XF, Xiang Y (2017) Numerical simulation of the effects of bypass current on droplet transfer during AZ31B magnesium alloy DE-GMAW process based on FLUENT. *Int J Adv Manuf Tech* 90(1–4):857–863. <https://doi.org/10.1007/s00170-016-9438-y>
  24. Ding XP, Li H, Yang LJ, Gao Y (2013) Numerical simulation of metal transfer process in tandem GMAW. *Int J Adv Manuf Tech* 69(1–4):107–112. <https://doi.org/10.1007/s00170-013-4999-5>
  25. Ma GH, Liu JC, Yu LS, Hong L, He YS (2019) Numerical simulation of droplet transfer process in ultrasonic-assisted MIG welding. *Sci Technol Weld Join* 25(3):1–11. <https://doi.org/10.1080/13621718.2019.1664540>

**Publisher's note** Springer Nature remains neutral with regard to jurisdictional claims in published maps and institutional affiliations.

Springer Nature or its licensor holds exclusive rights to this article under a publishing agreement with the author(s) or other rightsholder(s); author self-archiving of the accepted manuscript version of this article is solely governed by the terms of such publishing agreement and applicable law.